Progress In Electromagnetics Research, Vol. 119, 133–153, 2011

CALCULATION OF WHOLE-BODY SAR FROM A 100 MHz DIPOLE ANTENNA

M. Zhang* **and A. Alden**

Electromagnetics and Compatibility/Terrestrial Wireless Systems, Communications Research Centre Canada, 3701 Carling Avenue, Ottawa, Ontario K2H 8S2, Canada

Abstract—This paper presents results of a dosimetry study at an FM broadcasting frequency of 100 MHz. The work focused on SAR calculations with high resolution Magnetic Resonance Imaging (MRI)-based full-body models. FDTD computer modeling used a half-wave dipole as the exposure source. Extensive calculations give the variation of SAR with distance and show that whole-body average SAR exhibits a different distance dependency from the incident power density. Body size has a significant effect on SAR. Based on the numerical results, an empirical formula was developed to describe the relationship between antenna input power and distance for the limiting SAR value.

1. INTRODUCTION

This paper investigates health concerns from human exposure to RF communication antennas. Exposure is usually measured in terms of the specific absorption rate (SAR), which is the time derivative of dissipated energy per unit mass within the exposed body caused by the incident electromagnetic fields. Specifically, SAR is defined as the power absorbed per unit mass of tissue, usually averaged either over the whole body or over a small sample volume (typically 1 g or 10 g of tissue). Safety guidelines for limiting electromagnetic field exposure have been published by the International Commission on Non-Ionizing Radiation Protection (ICNIRP) [1] and the Institute of Electrical and Electronics Engineers (IEEE) [2]. In most countries, these guidelines have been adopted as the basic limits on SAR, to prevent adverse health effects related to whole-body heat stress and excessive localized tissue heating for frequencies between 3 kHz and 300 GHz.

Received 20 May 2011, Accepted 2 July 2011, Scheduled 24 July 2011

* Corresponding author: Ming Zhang (ming.zhang@crc.gc.ca).

Accurate RF dosimetry measurements in simulated whole bodies are complex. They require fabricated phantom models with various tissue geometries and specially developed liquids for tissue-equivalent materials, and a robot fitted with a measurement probe [3–6]. Various numerical simulation techniques are now available and provide alternative effective methods to determine SAR distributions in highly sophisticated millimeter-resolution anatomically based models. Among those techniques, the finite-difference time-domain (FDTD) method has become the most widely used method for bio-electromagnetic applications [7–11].

In a previous study [12], a direct relationship was established between RF power density from mobile base station antennas and specific absorption rate (SAR). Empirical formulas were developed to predict the variation of SAR values with distance, frequency and antenna pattern. Analyses relating the SAR limit and the compliance distance, were carried out using these formulas. To our knowledge, full-body calculations of SAR with distance at FM frequencies, are not available in the literature. The current paper is specific to calculations at a broadcasting frequency of 100 MHz.

In order to investigate the direct relationship between transmitted power and SAR, a free-space scenario has been considered, in which the incoming radio signal is in a line-of-sight path to a stationary human body, with no surrounding structures, trees etc. A free-space analysis permits an understanding of the basic processes involved. Later additions of suitable factors describing multipath, foliage attenuation etc. are then possible. A SAR analysis for a soil ground beneath the body models, has also been performed [13]. In the present paper, calculations have been performed as the body model was moved away up to 60 m from the antenna. At each location, whole-body average and peak spatial-averaged SAR values over 1- and 10-g mass were evaluated in accordance with IEEE Standard C95.3-2002 (R2008) [14].

The paper is organized as follows:

Section 2 gives brief descriptions of the anatomical full-body models, FM broadcasting antenna, the electromagnetic simulation tool, and computer simulation setup used in this study.

Simulation results are presented in Section 3. Whole-body average and peak spatial-averaged SAR values over 1- and 10-g mass are calculated as the body is moved away from the antenna. Locations of tissues with peak spatial-averaged SAR values are determined.

In Section 4, based on the numerical study, an empirical formula is developed to describe the variation of SAR values with horizontal distance. With this formula, compliance analyses can be carried out.

In Section 5, representative results for a soil ground, are given,

while in Section 6, conclusions and discussions are presented.

2. NUMERICAL MODELS AND COMPUTER MODELING

For the simulations, two full-body Magnetic Resonance Image (MRI)-based models, from the ITIS foundation [15], were used. The MRI models have 84 different tissues and organs. The male adult and 11-year-old girl models have heights and weights of 1.81 and 1.46 m and 71.5 kg and 35.0 kg, respectively. These two models are shown in Figure 1. Model dimensional specifications are given for individuals in a supine position. When rotated to the vertical, body length from the ground is larger than true height because the lying-down position of the feet during dimensional measurements translates to a tip-toe position in the vertical.

Frequency dependence of the electromagnetic parameters of body tissues is described using the Gabriel Cole-Cole analysis [16], and

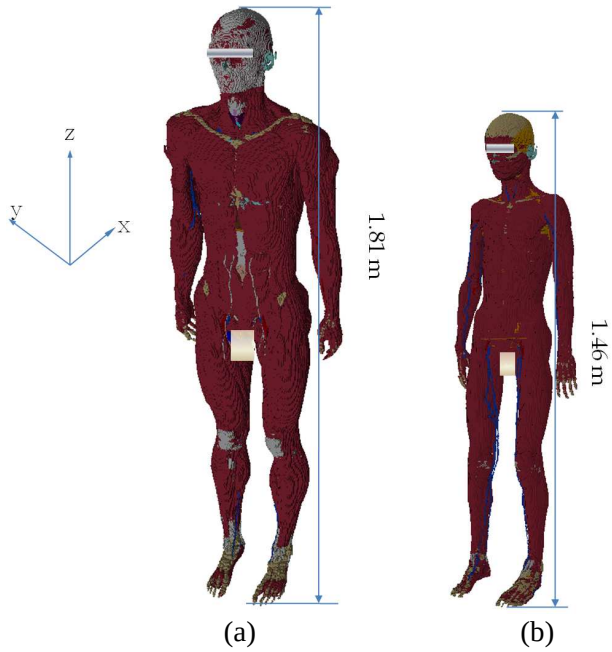

Figure 1. The MRI full-body anatomical models used in this study (a) a 71.5-kg adult male (name: Duke), (b) a 34.8-kg 11-year old girl (name: Billie).

calculated with FDTD-based software from Empire [17]. Excellent agreement is obtained between these calculated parameters and values from the Italian National Research Council [18] and FCC web pages [19].

A standard half-wave dipole antenna was used as the exposure source for this study. Figure 2 summarizes the radiation characteristics of the antenna, together with the far-field radiation pattern at 100 MHz. The radiated field distribution of this antenna at 100 MHz is believed typical of FM antennas designed for centre frequencies in the range 88–108 MHz.

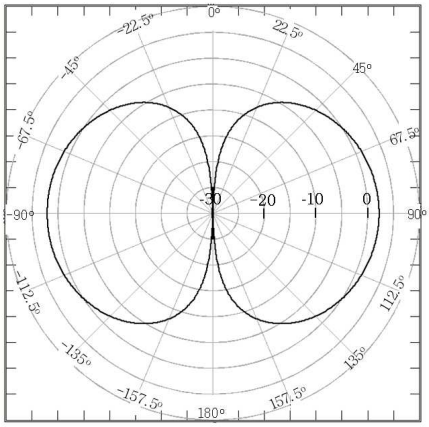

Figure 2. *E*-plane radiation pattern at 100 MHz and summary of the radiation characteristics of the FM dipole antenna.

As mentioned, a scenario is considered, in which the incoming radio signal is in a line-of-sight path to a stationary human body in free space. In simulations, the two body models were, in turn, positioned facing the antenna. The lower extremity of the antenna was fixed at 0.15 m above body height (H_b = 0.15 m). SAR calculations were performed as the body model was moved up to 60 m from the antenna. Figure 3 illustrates this scenario.

An important issue is computational domain meshing. A rule of thumb requires at least 10 meshes per wavelength. In our simulations, different meshing schemes have been applied for the inside and outside of the body. Inside the body, the largest relative dielectric constant (Kidneys) is 98.01 at 100 MHz, and the shortest wavelength (λ_g) is

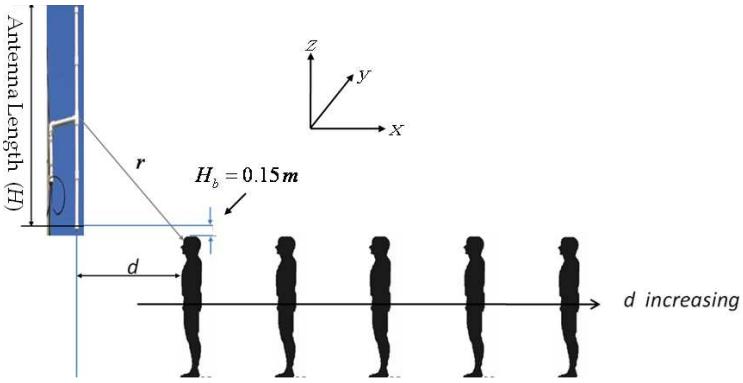

Figure 3. The simulation boundary condition setup: A resistive sheet boundary with an air intrinsic impedance of 377 Ω was applied to the $+z$ computational domain wall; 6-layer perfectly matched layer boundary conditions have been applied to the other five walls (the $\pm x$, $\pm y$ and $-z$ walls).

thus approximately 0.3 m. However, the mesh size is chosen to match the 'cell' dimension used for the MRI body description, namely 2 mm. This is the voxel size used for both models, small enough to meet all accuracy requirements. Outside the body, variable mesh sizes are used with a maximum of $\lambda_o/10$ (λ_o is the free-space wavelength). SAR calculations have been performed according to IEEE Standard C95.3-2002 (R2008) [14]. Iteration and interpolation techniques are employed to obtain 1- or 10-g of tissue mass, and peak-spatial and average SAR values.

The convergence of the numerical solution has been verified by checking the behaviour of calculated reflection coefficients, input impedance and stability of simulations over the operating range of 90–105 MHz. Experimentations have included increasing the number of simulation timesteps, and reducing the maximum energy level (left inside the structure) to a minimum of −80 dB [17].

3. NUMERICAL RESULTS

Whole-body average SAR values over 1- and 10-g mass have been calculated as each model was moved away from the antenna. All results are for antenna input power normalized to 1 W, unless otherwise mentioned. Using the maxima location feature and voxel editor of the Empire Software, peak spatial-averaged SAR values and their tissue locations were obtained.

3.1. Results for Whole-body Average SAR

The body models were first placed almost under the antenna ($d = 0.10\,\text{m}$) and gradually moved out to 60 m. Less than 0.1% difference in SAR values was noted between whole-body average SAR calculations over 1- and 10-grams of tissue. Whole-body average SAR values for the adult male and girl models are plotted as a function of slant distance r, in Figure 4. From Figure 3, the slant distance r at a separation of d is

$$r = \sqrt{d^2 + \left(\frac{H}{2} + H_b\right)^2} \tag{1}$$

where H is the antenna length, and H_b the vertical separation from the lower end of the antenna to the top of the head. Energy deposition within a real body in the near- field and transition regions may be more closely related to power in the incident wave at head height rather than at any other single body location. Far-field data are essentially independent of the single body location chosen. Thus, comparison between SAR simulations for differing body models and variations with distance, were felt more meaningful with such a definition of slant (reference) distance. It is seen that SAR values for the adult male model are lower than those for the girl by a factor of approximately 2.

For $r \leq H$, a complex situation exists with significant near-field incident wave distributions downward on the head and upper

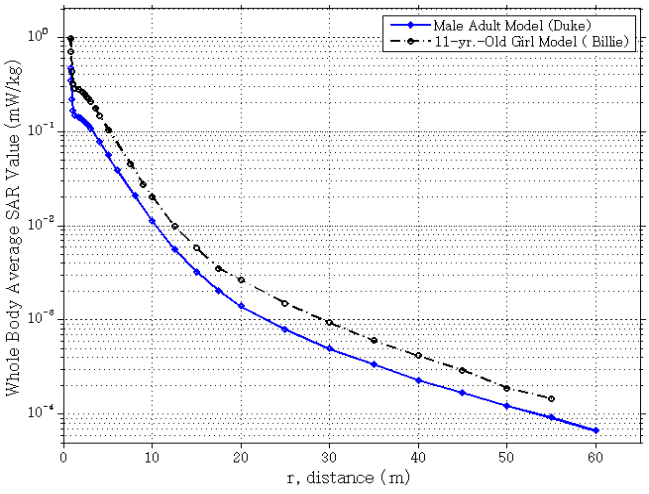

Figure 4. Whole-body average SAR values versus body-antenna slant distance r, for body models exposed to the antenna at 100 MHz.

torso. Far-field incidence on the lower torso is negligible. An analysis requires, at the very least, a lossy dielectric waveguide model for body slab geometry with coupling mechanisms for incident electric field components parallel to orthogonal waveguide faces. This is presently under development. It can however, be said at this stage that with the near-field waves incident on the top and variable part of the front sides, the 'resonant' phenomena described below for far-field contributions, may well be largely absent.

Contributions to differences in SAR values can also be attributed to tissue compositions. Fat and muscle are the two most significant tissues in terms of their amounts and volumes. Fat and muscle compositions are around 1.2% and 7.1% for the girl model, and 2.6% and 10.8% for the man model, respectively. Thus fat-to-muscle ratios are different. Analysis has shown [20] that whole body average SAR is significantly dependent on subcutaneous fat. At RF frequencies above body resonance, a statistically thicker fat layer behaves as an impedance matching layer between the external free space and the internal lossy tissues, resulting in larger SAR values [20, 21].

For $r > H$, far-field conditions obtain, with the body moving further into a broadside wave incidence. As mentioned above, this may be modeled as a lossy dielectric waveguide antenna with field coupling and parameters that are functions of the dimension along the electric field direction. The increase in child SAR over adult in the far-field, is supported by numerical results in the literature [22]. These describe a 'resonance' phenomenon for body heights of $0.4\lambda_o$ [23]. This corresponds closely to the girl model height at 100 MHz.

A uniformly lossy dipole model for the human body has been used in [24] to estimate body currents. Ohmic losses (SAR) are then readily calculated from the integral of body currents squared. From this receive dipole model, SAR for the girl is found to be around nine times that for the adult male. This discrepancy supports the need for a dielectric receive antenna model.

3.2. SAR Variation with Distance

To further examine the behaviour of SAR with distance, SAR values as a function of distance, Figure 4, have been re-plotted on a logarithmic-decibel scale. These are presented as Figures 5 and 6 for the adult male and girl models, respectively. In these two Figures, the behaviour of SAR can be characterized by three distinct intervals of slant distance. The first interval is the near-field from the closest distance to $r \approx H$ (Antenna Length = 1.34 m). In the second interval, SAR decays at a slower rate until the models are 'fully' into broadside wave incidence

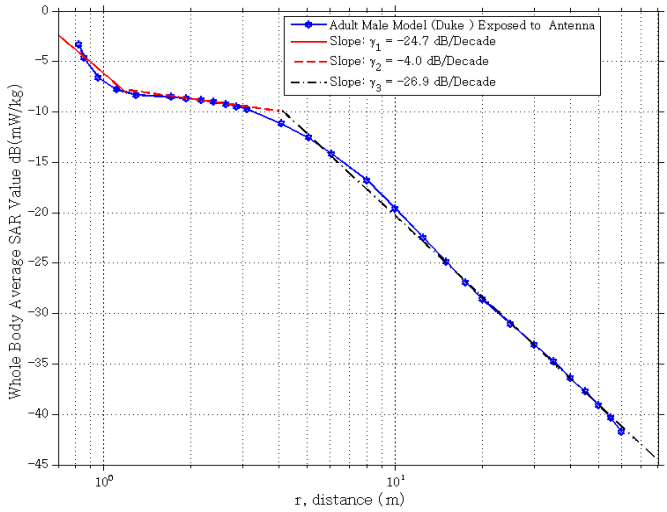

Figure 5. Whole-body average SAR values versus body-antenna slant distance r at 100 MHz, plotted in logarithmic-decibel scale, for an adult male model (Duke).

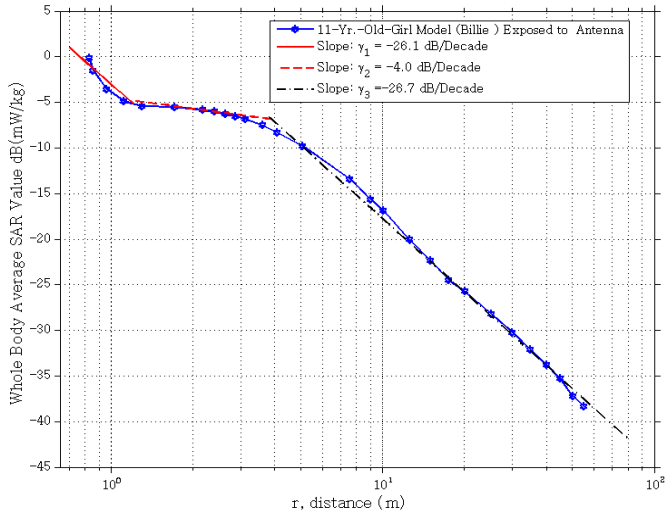

Figure 6. Whole-body average SAR values versus body-antenna slant distance r at 100 MHz, plotted in logarithmic-decibel scale, for an 11-year-old girl model (Billie).

(far-field pattern). The end location of this transition interval is at approximately 4.0 m.

A linear fit has been used in the logarithmic scale coordinate system, and three piecewise approximate expressions obtained for the intervals, also shown in Figures 5 and 6. In each interval, variation of SAR with distance is expressed as an exponential function of distance by using a path slope, that is, the dependency of SAR with distance can be described as $1/r^{\gamma}$. The slopes γ were found as $\gamma_1 = 2.47$ and 2.61, $\gamma_2 = 0.40$ and 0.40 and $\gamma_3 = 2.69$ and 2.67 in the three sequential intervals, for the adult male and girl models, respectively. SAR values are thus seen to have different distance dependencies to the incident power density. In a recent work [25], a formula was proposed to estimate whole-body SAR from RF exposure to base station antennas. In this reference, SAR was assumed to have the same distance dependency as the incident power density. Based on this assumption, SAR should decay as $1/r^2$ in the far field. From their results [25], this formula is a significant overestimate, and not suitable for practical assessment purposes. Current calculations at Wi-Fi frequencies also support a different distance dependency from the incident power density [26].

The same dependency of SAR and incident power with distance, is only predicated for EM fields which remain identical, to within the resolution of the receiving system (2 mm). This is not the case for the fields of a dipole antenna, except at large distances beyond the concerns of this study. The slope of SAR with far-field distance has been found to vary with details of dipole beam deviation from uniformity, and is under continuing investigation.

For a dielectric waveguide model of the body [13], the 'top' plane (top of the head and shoulders) and 'front' plane (front of the torso) are considered entry regions for energy transportation and deposition within the body. Within Interval 1, the head and front upper torso remain in the dipole near-field. In Interval 2 (transition region), the entire body is in the dipole far-field and the far-field radiation pattern is critical. At the near-field boundary, power entry through the front of the torso is relatively small. As the distance increases within the transition region, the front of the body comes closer to the dipole beam broadside direction, where incident radiation is a maximum. Thus, although a drop off in SAR is expected because of increased distance from the antenna, this is also expected to be partly or even fully compensated by an increase in antenna radiation as the incidence angle approaches the broadside condition. The choice of the 60% power points permits a good fit to the data. That is, once the body is entirely within, or close to, the 60% power points of the beam, the averaged

increase in incident power radiation with distance diminishes quickly, and radiation power density drop off becomes the overriding factor for SAR variations. That is, in Interval 3 (far-field), beam incursion is essentially complete, and an approximately constant $1/r^{\gamma}$ fall off in SAR is expected.

3.3. Peak Spatial-averaged SAR

At each horizontal distance d, peak spatial-averaged SAR for the whole body was calculated, over 1 g and 10 g. Locations of tissue with peak values were determined with the voxel editor. Tables 1 and 2 summarize these values and horizontal locations for the two body models. Examples of the SAR distributions for the adult male and girl models, on a cross-section with peak values, are presented in Figures 7 and 8.

The results in Table 1 and Table 2 show that: (1) peak SAR values averaged over 1 g are larger than those over 10 g, as expected.

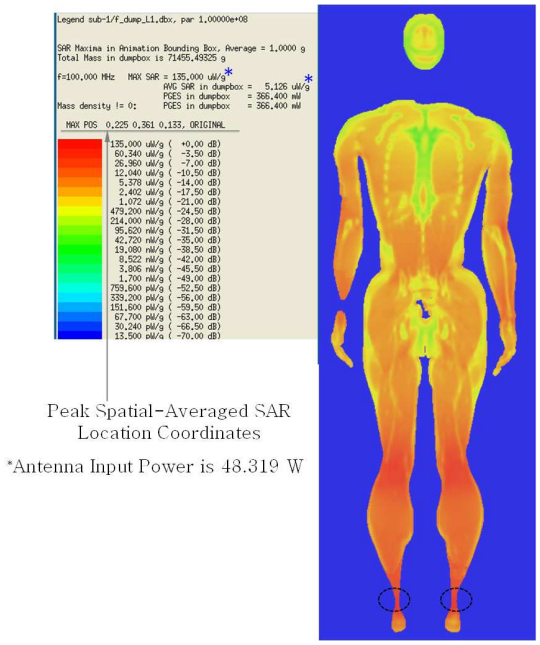

Figure 7. SAR value distribution (2 mm mesh size) for the adult male model (Duke), on a cross-section with peak value at $d = 3.0$ m, in which the locations of peak spatial-averaged SAR values are circled on the ankles.

Table 1. Location of tissues with peak spatial-averaged SAR values of an adult male model (Duke) at 100 MHz.

d Horizontal Distance (m)	Peak Spatial-Averaged SAR values (W/kg) and Location of Tissues, over 1g-mass	Peak Spatial-Averaged SAR values (W/kg) and Location of Tissues, over 10g-mass
0.10	10.9933×10^{-3}/Tendon-Ligament (Ankle)	5.5341×10^{-3} / Fat (Ankle)
0.25	8.3926×10^{-3} / Tendon-Ligament (Ankle)	4.2212×10^{-3} / Fat (Ankle)
0.50	5.3501×10^{-3} / Tendon-Ligament (Ankle)	2.6854×10^{-3} / Fat (Ankle)
0.75	3.9079×10^{-3} / Skin (Ankle)	2.0091×10^{-3} / Fat (Ankle)
1.00	3.4188×10^{-3}/ Skin (Ankle)	1.7828×10^{-3} / Fat (Ankle)
1.50	3.3707×10^{-3} / Tendon-Ligament (Ankle)	1.7044×10^{-3} / Fat (Ankle)
1.75	3.3873×10^{-3}/ Tendon-Ligament (Ankle)	1.6883×10^{-3} / Fat (Ankle)
2.00	3.3463×10^{-3} / Skin (Ankle)	1.6690×10^{-3} / Fat (Ankle)
2.25	3.2434×10^{-3} / Tendon-Ligament (Ankle)	1.6180×10^{-3} / Fat (Ankle)
2.50	3.1210×10^{-3} / Tendon-Ligament (Ankle)	1.5572×10^{-3} / Fat (Ankle)
2.75	2.9677×10^{-3} / Tendon-Ligament (Ankle)	1.4793×10^{-3} / Fat (Ankle)
3.00	2.7939×10^{-3}/ Tendon-Ligament (Ankle)	1.3920×10^{-3} / Fat (Ankle)
4.00	2.0025×10^{-3}/ Tendon-Ligam ent (Ankle)	1.0079×10^{-3} / Muscle (around Knee)
5.00	1.4059×10^{-3} Tendon-Ligament (Ankle)	0.7334×10^{-3} /Muscle (around Knee)
6.00	0.9463×10^{-3}/ Tendon-Ligam ent (Ankle)	0.5084×10^{-3} / Muscle (around Knee)
8.00	0.4823×10^{-3}/ Tendon-Ligament (Ankle)	0.2737×10^{-3} / Muscle (around Knee)
10.0	0.2404×10^{-3} / Tendon-Ligam ent (Ankle)	0.1415×10^{-3} / Muscle (around Knee)
12.5	0.1132×10^{-3} / Tendon-Ligam ent (Ankle)	0.0700×10^{-3} / Muscle(around Knee)
15.0	0.0605×10^{-3} / Tendon-Ligam ent (Ankle)	0.0397×10^{-3} / Muscle (around Knee)
17.5	0.0353×10^{-3}/ Tendon-Ligam ent (Ankle)	0.0242×10^{-3} / Muscle (around Knee)
20.0	0.0230×10^{-3} / Tendon-Ligam ent (Ankle)	0.0162×10^{-3} / Muscle (around Knee)
25.0	0.0123×10^{-3} / Vein (around Knee)	0.0090×10^{-3} / Muscle (around Knee)
30.0	0.0077×10^{3} / Vein (around Knee)	0.0056×10^{-3} / Muscle (around Knee)
35.0	0.0052×10^{-3} / Vein (around Knee)	0.0038×10^{-3} / Muscle (around Knee)
40.0	0.0035×10^{-3}/ Vein (around Knee)	0.0026×10^{-3} / Muscle (around Knee)
45.0	0.0026×10^{-3}/ Vein (around Knee)	0.0018×10^{-3} / Muscle (around Knee)
50.0	0.0019×10^{-3}/ Vein (around Knee)	0.0014×10^{-3} / Muscle (around Knee)
55.0	0.0014×10^{-3}/ Muscle (around Knee)	0.0010×10^{-3} / Muscle (around Knee)
60.0	0.0010×10^{-3}/ Vein (around Knee)	0.0007×10^{-3} / Muscle (around Knee)

Table 2. Location of tissues with peak spatial-averaged SAR values of a 11-year-old girl model (Billie) at 100 MHz.

d Horizontal Distance (m)	Peak Spatial-Averaged SAR values (W/kg) and Location of Tissues, over 1g-mass	Peak Spatial-Averaged SAR values (W/kg) and Location of Tissues, over 10g-mass
0.10	13.6934×10^{-3} /Muscle (around Knee)	7.9466×10^{-3}/ Muscle (around Knee)
0.25	10.005×10^{-3} /Muscle (around Knee)	5.9357×10^{-3}/ Muscle (around Knee)
0.50	6.123×10^{-3} / Muscle (around Knee)	3.7122×10^{-3}/ Muscle (around Knee)
0.75	4.3720×10^{-3} / Muscle (around Knee)	2.6734×10^{-3}/ Muscle (around Knee)
1.00	3.8408×10^{-3} / Skin (around Knee)	2.3179×10^{-3} / Skin (around Knee)
1.50	3.9612×10^{-3}/ Muscle (around Knee)	2.3260×10^{-3} /Muscle (around Knee)
2.00	3.8037×10^{-3}/ Muscle (around Knee)	2.2226×10^{-3} /Muscle (around Knee)
2.25	3.6915×10^{-3}/ Muscle (around Knee)	2.1262×10^{-3} /Muscle (around Knee)
2.50	3.5157×10^{-3} / Muscle (around Knee)	2.0127×10^{-3} /Muscle (around Knee)
2.75	3.3508×10^{-3} Skin (around Knee)	1.9119×10^{-3} / Skin (around Knee)
3.00	3.1250×10^{-3}/ Muscle (around Knee)	1.7719×10^{-3} /Muscle (around Knee)
3.50	2.6827×10^{-3}/ Muscle (around Knee)	1.5154×10^{-3}/ Muscle (around Knee)
4.00	2.2517×10^{-3}/ Skin (around Knee)	1.2468×10^{-3}/ Skin (around Knee)
5.00	1.5997×10^{-3} Muscle (around Knee)	0.8663×10^{-3} /Muscle (around Knee)
7.50	0.6993×10^{-3} / Muscle (around Knee)	0.3618×10^{-3} / Muscle (around Knee)
9.00	0.4124×10^{-3} / Muscle (around Knee)	0.2088×10^{-3}/ Muscle (around Knee)
10.0	0.2998×10^{-3} Muscle (around Knee)	0.1596×10^{-3}/ Muscle (around Knee)
12.5	0.1477×10^{-3} Muscle (around Knee)	0.0716×10^{-3}/ Muscle (around Knee)
15.0	0.0856×10^{-3}/ Muscle (around Knee)	0.0401×10^{-3} /Muscle (around Knee)
17.5	0.0515×10^{-3} / Muscle (around Knee)	0.0234×10^{-3}/ Muscle (around Knee)
20.0	0.0387×10^{-3} / Muscle (around Knee)	0.0171×10^{-3} /Muscle (around Knee)
25.0	0.0219×10^{-3}/ Muscle (around Knee)	0.0097×10^{-3} /Muscle (around Knee)
30.0	0.0145×10^{3} / Muscle (around Knee)	0.0061×10^{-3} /Muscle (around Knee)
35.0	0.0087×10^{-3} Muscle (around Knee)	0.0039×10^{-3} /Muscle (around Knee)
40.0	0.0060×10^{-3}/ Muscle (around Knee)	0.0027×10^{-3} /Muscle (around Knee)
45.0	0.0041×10^{-3}/ Muscle (around Knee)	0.0018×10^{-3} /Muscle (around Knee)
50.0	0.0028×10^{-3}/ Muscle (around Knee)	0.0012×10^{-3} /Muscle (around Knee)
55.0	0.0022×10^{-3}/ Muscle (around Knee)	0.0010×10^{-3} /Muscle (around Knee)

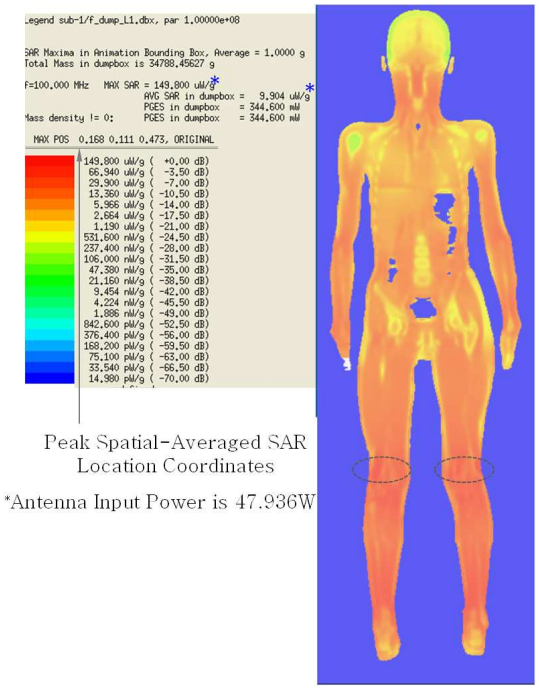

Figure 8. SAR Value Distribution (2 mm mesh size) for the 11-year-old girl model (Billie), on a cross-section with peak value at $d = 3.0$ m, in which the locations of peak spatial-averaged SAR values are circled on the knees.

(2) Tissues with peak SAR values occur in the ankle or knee. In a similar fashion to that discussed in [25] for whole-body SAR, local SAR levels vary approximately inversely with the average depth of local cross-sections. The lower body has a smaller average depth than other parts of the body.

4. ESTIMATION OF SAR EXPOSURE FROM FM ANTENNA

An important aspect of this study was to develop an estimation formula, which can be used to calculate whole-body average SAR at FM radio frequencies for a range of antennas and scenarios, and is easy to use for practical assessment purposes. An FM broadcast antenna operates at a fixed frequency. A half-wave dipole design is typically used at the frequency of transmission, to simplify matching

and maximize power. The radiation characteristics of half-wave dipoles are well known, and depend upon the relative electrical length rather than the actual frequency. In addition, emphasis in the present paper is on dipole/body model interactions and the procedures for estimation formulas. These interaction processes are not expected to vary in type over the narrow FM band of 88–108 MHz, though changes in SAR up to about 60% will occur for a range of body models [22]. In the previous Section, simulations were carried out to evaluate the variations of SAR with distance. The behaviour of SAR with distance is very resistant to analytical treatment, and numerical techniques must be employed.

As mentioned, the behaviour of SAR with distance is characterized by three distinct intervals. The first interval is from the closest distance to $r \approx H$, the second interval starts at this location, with a gradual transition until a distance r_f is reached, and the third interval is from r_f. The transition distance r_f is defined as the slant distance to the top of the model head such that the entire body (of height H_m) is within the 60% power points of the far-field beam. Specifically, the feet of the model are on the 60% power beamwidth point θ_{60}. From Figure 9, the distance r_f is given by

$$r_f = \sqrt{d_f^2 + (H/2 + H_b)^2} \tag{2}$$

where

$$d_f = (H_m + H_b + H/2)\cot\theta_{60} \tag{3}$$

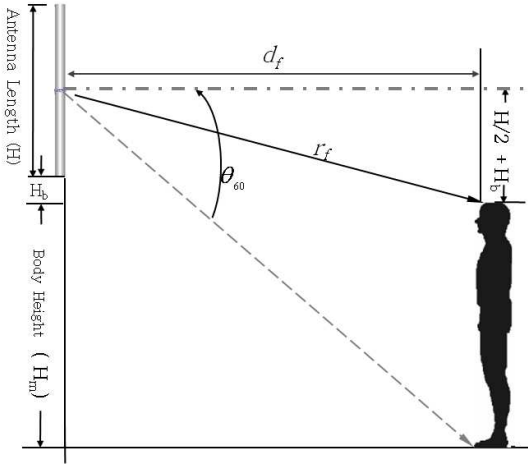

Figure 9. Transition distance and the power beamwidth of the antenna.

For the present scenario, this gives transition distances of 4.0 and 3.7 m for the adult male and girl models, respectively.

Using the linear slope expressions developed in Section 3, the proposed general estimation formula for whole-body average SAR is

$$SAR_{Ave}(r, P_{in}, D_o, \Phi) = \begin{cases} b_1 \chi \frac{P_{in}}{r^{\gamma_1}} & r_{\min} \le r \le H \\ b_2 \chi \frac{P_{in}}{r^{\gamma_2}} \frac{1}{\left(\Phi/\Phi_o\right)} & H \le r \le r_f \\ b_3 \chi \frac{P_{in}}{r^{\gamma_3}} \frac{D_o}{D_o^{\lambda/2}} \frac{1}{\left(\Phi/\Phi_o\right)} & r_f \le r \end{cases} \quad (4)$$

where r = slant distance from the centre of the antenna to the body head. $r_{\min}$ = the closest slant distance $r_{\min}$ from the antenna = 0.83 m (the closest horizontal distance $d_{\min} = 0.1$ m) for this study. b_1, b_2 and b_3 are constants found in the next page. P_{in} = input power. In the previous Section, it is normalized to 1 W. D_o = directivity of antenna and $D_o^{\lambda/2} = 1.636$ (Half-wavelength dipole used in this study). Φ = antenna vertical half-power beamwidth/2, $\Phi_o = 52^\circ$ (for the dipole used in this study). χ = size factor to accommodate different body models, $\chi = 1$ and 2 for the adult male and girl models, respectively. γ_1, γ_2 and γ_3 are slope values numerically defined, γ_1 for the near-field, γ_2 for the near-to-far-field transition interval, and γ_3 for the far-field, averaged over the two body models.

$$\gamma_1 = 2.51, \quad \gamma_2 = 0.41 \quad \text{and} \quad \gamma_3 = 2.68 \quad (5)$$

A direct relationship between maximum power and the SAR limit can be established for compliance with safety guidelines [1, 2]. Let $P_{in} = P_c$ be the required input power to produce the SAR limit at the slant compliance distance r_c, that is,

$$SAR_{Ave}^{\lim} = SAR\,(r_c, P_c, D_o\,, \Phi). \quad (6)$$

Using Equations (1) (Section 3.1), (4) and (6), the power-horizontal distance compliance relationship can be obtained as:

$$d_c = \begin{cases} \sqrt{\left(b_1 \chi \frac{P_c}{SAR_{Ave}^{\lim}}\right)^{2/\gamma_1} - (\frac{H}{2} + H_b)^2}, & P_o \le P_c < P_1 \\ \sqrt{\left(\frac{b_2 \chi}{(\Phi/\Phi_o)} \frac{P_c}{SAR_{Ave}^{\lim}}\right)^{2/\gamma_2} - (\frac{H}{2} + H_b)^2}, & P_1 \le P_c \le P_f \\ \sqrt{\left(\frac{b_3 \chi}{(\Phi/\Phi_o)} \frac{P_c}{SAR_{Ave}^{\lim}} \frac{D_o}{D_o^{\lambda/2}}\right)^{2/\gamma_3} - (\frac{H}{2} + H_b)^2}, & P_c > P_f \end{cases} \quad (7)$$

where $SAR_{Ave}^{\lim} = 0.08\,\mathrm{W/kg}$, a whole body SAR limit for devices used by the general public. b_1, b_2 and b_3 are chosen to give a good fit to horizontal compliance distance numerical data

$$b_1 = 3.0 \times 10^{-4}, \quad b_2 = 2.0 \times 10^{-4} \quad \text{and} \quad b_3 = 5.5 \times 10^{-3} \tag{8}$$

P_o = required input power to produce the SAR limit value at the closest slant distance $r_{\min}$.

$$P_o = \frac{SAR_{Ave}^{\lim} r_{\min}^{\gamma_1}}{b_1 \chi} \tag{9}$$

P_1 = required input power to produce the SAR limit value at the near-field/far-field boundary, $r_H \approx H$ (antenna length).

$$P_1 = \left(\frac{\Phi}{\Phi_o}\right) \frac{SAR_{Ave}^{\lim} (r_H)^{\gamma_2}}{b_2 \chi} \tag{10}$$

P_f = required input power to produce the SAR limit value in the far-field at the transition point r_f.

$$P_f = \left(\frac{\Phi}{\Phi_o}\right) \frac{SAR_{Ave}^{\lim} (r_f)^{\gamma_3}}{b_3 \chi} \frac{D_o^{\lambda/2}}{D_o} \tag{11}$$

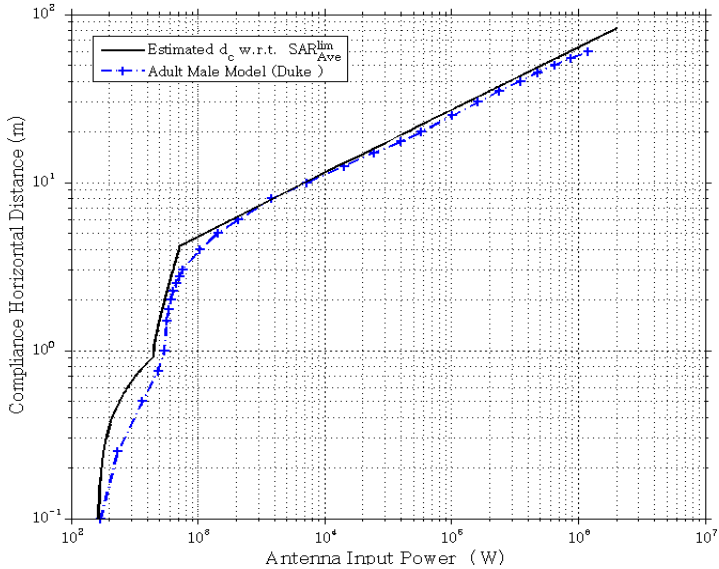

Figure 10. Compliance distances for an adult male model versus the antenna transmitted power. Black solid lines represent the estimated values.

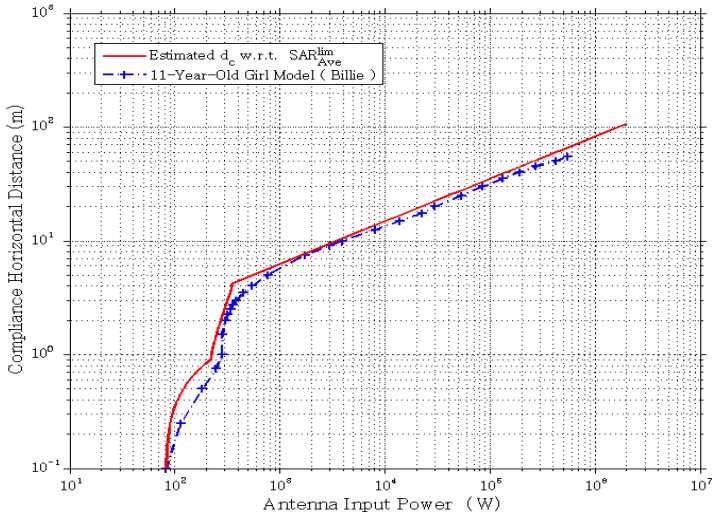

Figure 11. Compliance distances for an 11-year-old-girl model versus the antenna transmitted power. Red solid lines represent the estimated values.

Using Equations (5), (7) to (11), compliance distances were calculated, and shown in Figures 10 and 11 for the adult male and girl models, respectively, together with numerical data. Directivity, beamwidth and length of antennas have been considered in these Equations, and thus compliance formulas are applicable to any small single antenna. Body size factors χ used here are only accurate for the adult male and 11-year-old girl models. This factor, and hence compliance distance, will vary with other-size models. The results presented in this paper are not intended as worst-case data with respect to all body types.

5. SAR VALUES FOR A SOIL GROUND

To examine the effect of soil on SAR values, a 45 cm thick good-soil layer ($\varepsilon_r = 15$, $\sigma = 15$ mS) has been added, with a maximum width of 13.0 metres and bounded by perfectly matched layer (PML) boundary conditions.

Results for the 11-year-old girl model are presented in Figure 12. Simulation data without soil are also displayed. This Figure shows that in the far-field region, for $r > 5$ m, with a soil layer, SAR values decay with distance at a rate approximately ten-times slower than those without soil. Significant difference in SAR values with and without

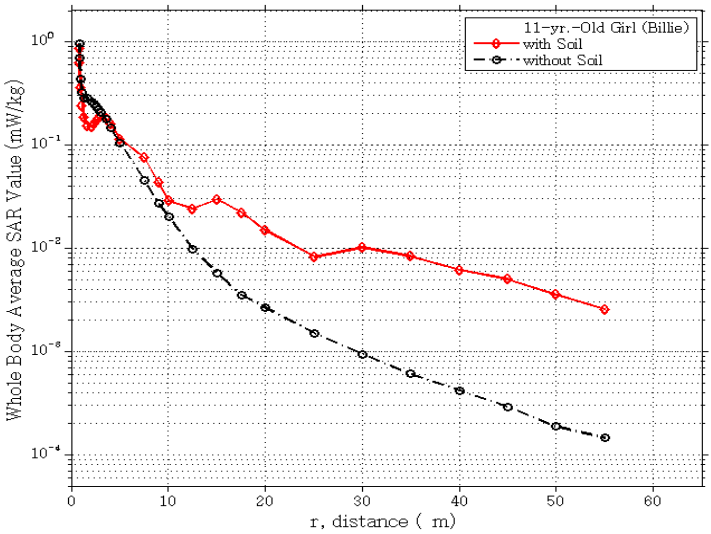

Figure 12. SAR values for the 11-year-old girl (Billie) with and without a soil layer.

a soil layer is caused by reflections from the soil layer and subsequent additions of the power in each wave in the body. A more detailed discussion is given in [13].

6. SUMMARY AND DISCUSSION

This paper establishes a direct relationship between RF maximum power density and the specific absorption rate (SAR) for exposure to FM radio broadcasting. An empirical formula has been developed to predict the variation of SAR values with distance, antenna transmitted power and pattern. Compliance analysis (SAR limit and compliance distance), can be carried out using the formula.

The work used FDTD computer modeling, with a single dipole antenna at 100 MHz as the exposure source. Full-body anatomical models were used for simulation of RF energy deposition. The models are Magnetic Resonance Image (MRI)-based models with 84 different tissues and organs.

For the calculations, a free-space scenario is used, in which the incoming radio signal is in a line-of-sight path to a stationary human body, with no supporting or surrounding structures, trees etc.. This permits a study of direct beam/body-model interactions in the near- and far- fields, prior to an interpretation of complex reflection effects

on a real beam, and resulting changes in SAR, see Section 5 and [13]. The dipole antenna was placed facing the body model, at 0.15 m above the body head. Simulations were carried out for the positioning of each body model, in turn, under the antenna, and at horizontal separations up to 60 m. Whole-body average SAR values over 1- and 10-g mass have been calculated according to IEEE Std. C95.3-2002 (R2008). Using the maxima location feature and voxel editor of the Empire FDTD program, peak spatial-averaged SAR values and their tissue locations were obtained.

Using the numerical results, an exponential function of distance was used to fit whole-body average SAR data in each of three intervals of operation, the near-field, the 'transition' region, and the far-field. In the far-field, SAR decays significantly faster than $1/r^2$.

Analyses have mainly focused on whole-body average SAR. Some aspects worthy of further work, are (1) Analyses of peak spatial-averaged SAR values and their tissue locations with currently available simulation data. These analyses will involve compliance with limits [2]; (2) Perform predictions of compliance distance in terms of other reference levels of exposure (field strength and power density) [2], and examine the consistency among the different reference levels; (3) Additional adult and child models are to be obtained to investigate the variability of SAR with body size and morphology; (4) Simulations will be carried out for the dipole at other heights above the body model to verify the applicability of the formulas, particularly in the near-field and transition regions; (5) Other antenna types will be used, to investigate the variability with antenna design and size.

REFERENCES

1. ICNIRP, "Guidelines for limiting exposure to time-varying electric, magnetic, and electromagnetic fields (up to 300 GHz)," *Health Phys.*, Vol. 74, 494–522, 1998.
2. "IEEE standard for safety levels with respect to human exposure to radio frequency electromagnetic fields 3 kHz to 300 GHz," IEEE Std. C95.1, 2005.
3. Wang, J., M. Fujita, O. Fujiwara, K. Wake, and S. Watanabe, "Uncertainty evaluation of an in vivo near-field exposure setup for testing biological effects of cellular phones," *IEEE Trans. Electromagn. Compat.*, Vol. 48, No. 3, 545–551, Aug. 2006.
4. Chou, C., H. Bassen, J. Osepchuk, Q. Balzano, R. Petersen, M. Meltz, R. Cleveland, J. Lin, and L. Heynick, "Radio frequency electromagnetic exposure: Tutorial review on experimental dosimetry," *Bioelectromagnetics*, Vol. 17, No. 3, 195–208, 1996.

5. Wang, J., O. Fujiwara, S. Kodera, and S. Watanabe, "FDTD calculation of whole-body average SAR in adult and child models for frequencies from 30 MHz to 3 GHz," *Phys. Med. Biol.*, Vol. 51, No. 3, 4119–4127, Aug. 2006.
6. Kawamura, Y., T. Hikage, and T. Nojima, "Experimental whole-body averaged SAR estimation system using cylindrical scanning method," *2009 International Symposium on Electromagnetic Compatibility*, 257–260, Kyoto, Japan, Jul. 2009.
7. Dimbylow, P. J. and S. M. Mann, "SAR calculations in an anatomically based realistic model of the head for mobile communication transceivers at 900 MHz and 1.8 GHz," *Physics in Medicine*, Vol. 39, 1537–1553, 1994.
8. Chen, J.-Y. and O. P. Gandhi, "RF currents induced in an anatomically-based model of a human for plane-wave exposures 20–100 MHz," *Health Physics*, Vol. 57, 89–98, 1989.
9. Allen, S. J., E. R. Adair, K. S. Mylacraine, W. Hurt, and J. Ziriax, "Empirical and theoretical dosimetry in support of whole body radio frequency (RF) exposure (100 MHz) in human volunteers," *Bioelectromagnetics*, Vol. 24, 502–509, 2003.
10. Allen, S. J., E. R. Adair, K. S. Mylacraine, W. Hurt, and J. Ziriax, "Empirical and theoretical dosimetry in support of whole body radio frequency (RF) exposure in seated human volunteers at 220 MHz," *Bioelectromagnetics*, Vol. 26, 440–447, 2005.
11. Lacroux, P. F., E. Conil, A. C. Carrasco, A. Gati, M. F. Wong, and J. Wiart, "Specific absorption rate assessment near a base-station antenna (2,140 MHz): Some key points," *Ann Telecommun.*, Vol. 63, 55–64, 2008.
12. Zhang, M. and W. Lauber, "Evaluation of RF exposure from mobile communication base station antennas," CRC Technical Memorandum, VPTWS-TM-09-10-01, Ottawa, Canada, Nov. 2009, (Internal Report upon Request).
13. Zhang, M. and A. Alden, "Evaluation of RF exposure from an FM (88–108 MHz) radio broadcasting antenna (Phase II study)," CRC Report, No. 2010-003, Ottawa, Canada, Dec. 2010.
14. "IEEE recommended practice for measurements and computations of radio frequency electromagnetic fields with respect to human exposure to such fields, 3 kHz to 300 GHz," IEEE Std. C95.3-2002, 2002.
15. Christ, A., et al., "The virtual family — Development of surface-based anatomical models of two adults and two children for dosimetric simulations," *Phys. Med. Biol.*, Vol. 55, Jan. 2010. Also High-resolution Whole-body Models at ITIS Foundation webpage:

http://www.itis.ethz.ch/index/index_humanmodels.html.

16. Gabriel, C., "Compilation of the dielectric properties of body tissues at RF and microwave frequencies," Brooks Air Force Tech. Rep. AL/OE-TR-1996–0037, 1996.
17. User's Manual for EMPIRE, Version 5.30, Nov. 008, at: http://www.empire.de/.
18. Tissue dielectric parameters provided by Italian National Council webpage at: http://niremf.ifac.cnr.it/tissprop/htmlclie/htmlclie.htm#stsftag.
19. Tissue dielectric parameters provided by FCC webpage at: http://www.fcc.gov/oet/rfsafety/ dielectric.html.
20. Sandrini, L., A. Vaccari, C. Malacarne, L. Cristoforetti, R. Pontalti, et al., "RF dosimetry: A comparison between power absorption of female and male numerical models from 0.1 to 4 GHz," *Phys. Med. Biol.*, Vol. 49, 5185–5201, 2004.
21. "National Council on Radiation Protection and Measurements, a practical guide to the determination of human exposure to radiofrequency fields," NCRP Report, No. 119, Bethseda, MD, 1993.
22. Conil, E., A. Hadjem, F. Lacroux, M. F. Wong, and J. Wiart, "Variability analysis of SAR from 20 MHz to 2.4 GHz for different adult and child models using finite-difference time-domain," *Phys. Med. Biol.*, Vol. 53, 1511–1525, Feb. 2008.
23. Electroherbalism, "Electrical and frequency effects on pathogens," at: http://www.electroherbalism.com/Bioelectronics/IntroductiontoBioelectronics/ElectricalandFrequencyEffectsonPathogens.htm.
24. King, R. W. P. and S. S. Sandler, "Electric fields and currents induced in organs of human body when exposed to ELF and VLF electromagnetic fields," *Radio Science*, Vol. 31, No. 5, 1153–1167, Sep.–Oct. 1996.
25. Thors, B., M. L. Strydom, B. Hansson, F. J. C. Meyer, K. Kärkkäinen, P. Zollman, S. ILvonen, and C. Törnevik, "On the estimation of SAR and compliance distance related to RF exposure from mobile communication base station antennas," *IEEE Trans. Electromagn. Compat.*, Vol. 50, No. 4, 837–848, Nov. 2008.
26. Zhang, M. and A. Alden, "Dosimetry study at Wi-Fi frequencies (Phase III study)," CRC Technical Report in Preparation, 2011.